Simple preparation of a sunshine -like bismuth oxyiodide nanosheets for photocatalytic degradation of organic pollutant under sunlight

F. K. Algethami[a], M. R. Elamin[a,b], B. Y. Abdulkhair[a,c*]
[a]Imam Mohammad Ibn Saud Islamic University (IMSIU), College of Science, Chemistry Department, Riyadh, KSA
[b]Industrial research and consultancy center (IRCC), Khartoum-North, Sudan
[c]Sudan University of Science and Technology (SUST), College of Science, Chemistry Department, Khartoum, Sudan

The spread of organic pollutants in water is encountering colossal problems worldwide, and it gets worst as the industry progresses. Among the suggested solutions, heterogenous photocatalysis was progressively applied to degrade organic pollutants. Herein, a simple ethylene glycol refluxing (EGR) method was optimized to fabricate bismuth oxyiodide (BiOI) nanoparticles with a percentage yield of 94.2%. The EGR method's success in preparing BiOI nanomaterial was confirmed by the results of X-ray diffraction, energy dispersive spectroscopy, and Fourier-transform-infrared spectroscopy. The scanning-electron-microscopy and the transmission electron microscopy analysis revealed that the sunshine-like nanosheets are composed of tiny nanoparticles. The BiOI was employed for photocatalytic degradation of organic pollutants under visible light. The adsorption capability of BiOI was investigated prior to its photocatalytic activity, and both investigations showed appealing results. The outcomes of this study nominated both the EGR method for fast preparation of a nanoscale BiOI and the applicability of BiOI as a photocatalyst to swap the organic pollutants from contaminated water using the free-inexhaustible sunlight.

1. Introduction

The spread of organic pollutants in all environmental components such as soil, air, and water is a tremendous challenge to humankind and all living organisms[1, 2]. The solubility of many organic compounds in water resulted in the contamination of water resources. Various industries such as textile, leather, and paper used dyes extensively [3-5]. Many techniques were employed to remove pollutants from water and wastewater, including adsorption, flocculation, ion exchange, and membrane methods [6-9]. The MG is considered a carcinogenic, mutagenic, and teratogenic organic pollutant. But still extensively used as dyeing material in textile, ceramics, and leather industries [10, 11]. MG poses a considerable threat to the environment. Therefore its elimination from water is of broad interest till now [12-18]. Adsorption is a popular method because of low-cost and ease of application, but it is just a reconcentration of pollutants requiring further incineration and/ or dumping.

The photocatalysis method is superior to the adsorption as the first includes both removal and decomposition of organic contaminants from water by radiant. The titanium oxide (TiO_2) and zinc oxide (ZnO) were investigated extensively as photocatalysts, but their activity was restricted to the narrow UV-region because of their relatively high energy-bandgap (2.9 - 3.2 eV) [19-23]. Recent studies focused on the utilization of the widely-ranged visible-region in photocatalytic processes. The Low bandgap-value of the bismuth oxyiodide (BiOI) (1.77 to 1.92 e.V) nominated it as an excellent candidate for visible light absorption and utilization for photocatalytic purposes

---

* Corresponding author: babiker35.by@gmail.com

[24]. Micro and nanoscale BiOI particles, plates, and sheets were obtained through different preparation routes such as hydrothermal, autoclave digestion, and solvothermal. Still, most of these methods included the time and energy-consuming autoclave digestion step [24-27]. This work targeted developing a simple process to prepare BiOI nanomaterial to be employed for the photodegradation of MG as a model of organic pollutants in water under natural sunlight.

2. Experimental

2.1. Materials
The ethylene glycol, bismuth nitrate pentahydrate ($Bi(NO_3)_3.5H_2O$), and potassium iodide (KI) were provided from the Sharlau-Spain while the malachite green dye was provided from LOBACHEM-India.

2.2. Synthesis of BiOI nanoparticles
0.0288 mol of ($Bi(NO_3)_3.5H_2O$) and 0.0577 moles of KI were dissolved in 200 ml ethylene glycol. The solution mixture was refluxed in a heating mantle for two hours, where a brick-red precipitate was formed. The mixture was cooled under ambient conditions to room temperature, diluted with 500 ml of distilled water, and filtered with a vacuum filteration system. The product was rinsed three times with 50 ml portions of distilled water, followed by three times 30 ml portions of ethanol. The moisture was evaporated from the product by placing it in an oven set at 105 ^{o}C for three hours, collected, and preserved in a container for further use.

2.3. Characterization of the as-prepared BiOI
The prepared BiOI was characterized by scanning electron microscopy (SEM)-JSM-IT300), transmission electron microscopy (TEM - accelerating voltage of 100 kV), X-ray diffraction (XRD, D8 Advance, Bruker, Billerica, USA), Brunauer-Emmett-Teller (BET) method (ASAP 2020 micromeritics Instrument Corp., Norcross, GA, USA), Fourier transform infrared spectroscopy (FTIR, Bruker TENSOR Series, Germany), and Uv-vis photoluminescence spectroscopy (Hitachi F-7000 Uv-vis photoelectron spectroscopy).

2.4. Adsorption study of BiOI
The adsorption was studied by adding 50 mg of the prepared BiOI to 200 ml of 10 mg.L^{-1} MG-solution. The mixture was stirred in darkness for 2h, within which 5 ml were withdrawn at 2, 4, 6,10, 20, 30, 60, and 120 min to investigate the adsorption kinetics.

2.5. Photocatalytic activity of BiOI
50 mg of BiOI were added to 200 ml of 10 mg.L^{-1} MG-solution. This mixture was stirred under natural sunlight, and 5 ml portions were withdrawn for 4h to explore the photocatalytic activity of the prepared BiOI towards MG. 200 ml of 10 mg.L^{-1} MG standard was stirred under the sunlight without the photocatalyst. The absorbance of MG was measured using UV-VIS-spectrophotometer (UV-VIS-D3500 LABOMED).

3. Results and discussion

3.1. Characterization
XRD analysis was employed to confirm the preparation of BiOl by the adapted method. As illustrated in Fig. 1a, the prepared BiOI showed high-intensity diffraction peaks at 2θ degrees of 29.55 and 31.56 that perfectly assigned to the plane (102) and (110) of BiOI, respectively. Besides, several diffraction peaks with medium or week intensities appeared at 9.53,19.25, 24.12, 33.05, 37.19, 39.19, 45.27, 46.39, 49.55, 51.18, 55.03, 59.84, 61.43, 65.35 and 65.98 that corresponds to the BiOI planes of (002), (011), (102), (110), (111), (103), (004), (200), (104), (005), (114), (212), (123), (115), (220) and (214) respectively; (ICDD 10-0445 and JCPDS 73-

2062). Concluded that the XRD pattern confirmed a tetragonal lattice structure for the BiOI.[28-30].

The elemental analysis of the sample was carried by EDS. The bismuth, oxygen, and iodide percentages in the as-prepared BiOI were 59%, 6%, and 34%, respectively. These findings were almost typical of the theoretical ratios of the elements in the BiOI.

Fig. 1b represents the FTIR vibration peaks for the as-prepared BiOI sample. The most abundant peaks between 390 cm-1 and 850 cm^{-1} could be assigned to the vibrations of the Bi–O, Bi-I, and O-I bonds of the BiOI. An adsorbed water caused the two vibration peaks at about 1620 and 3200 cm^{-1} that can be attributed to the O-H bending and stretching vibrations, respectively [31, 32]. The appearance of BiOI vibration peaks in this characteristic range reflected the successfulness of this method to prepare BiOI. Besides, the existence of adsorbed water revealed by IR analysis may justify the slite rise of oxygen percentage determined by EDS analysis.
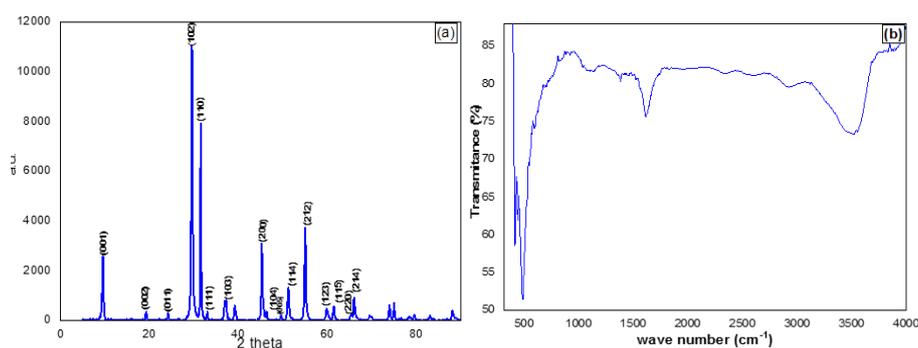
Fig. 1. (a) XRD pattern and (b) FTIR analysis for the prepared BiOI photocatalyst.

The surface and detailed morphology of BiOI was studied by SEM and TEM. The SEM presented nanosheets of BiOI having a sunshine-like configuration (Fig. 2a and b). On the other hand, the TEM results confirmed the nanosheets' presence with a thickness of less than 30 nm composed of BiOI nanoparticles of less than 20 nm size (Fig. 2c and d). Compared with the literature, BiOI nanosheets and nanoparticles prepared by this method present a smaller particle size [33-36].
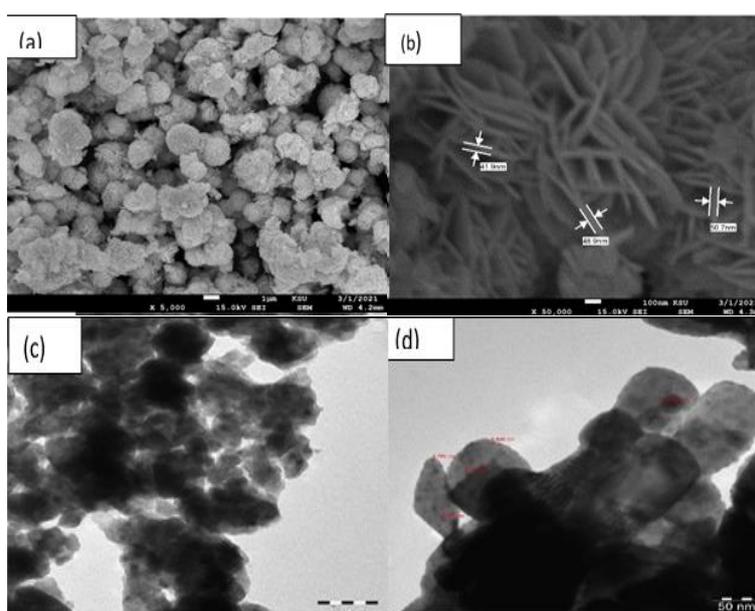
Fig. 2. (a)-(b) SEM results, and (c)-(d)TEM results for the prepared BiOI.

The porosity characteristics and surface area for the BiOI sunshine-like nanosheets were investigated by nitrogen adsorption-desorption methodology. Barrett-Joyner-Halenda (BJH) method was utilized to determine of the average pore volume (APV) and the average pore size (APS) for the prepared BiOI nanoparticles. In contrast, the BET method was used for the determination of the surface-area (Fig. 3a). The as-prepared BiOI nanoparticles showed H3- loop-type-hysteresis positioned in a relative pressure ranged between 0.05 to 1.0. The BET surface area, BJH-APV, and the BJH-APS were found to be 10.63 $m^2.g^{-1}$, 0.064 $cm^2.g^{-1,}$ and 25.62 nm, respectively. Fig. 3b revealed that the predominant pore-size ranged between 2.4 nm to 3.8 nm with a peak maximum at 2.95 nm, indicating the mesoporous nature of the prepared BiOI [37-42].
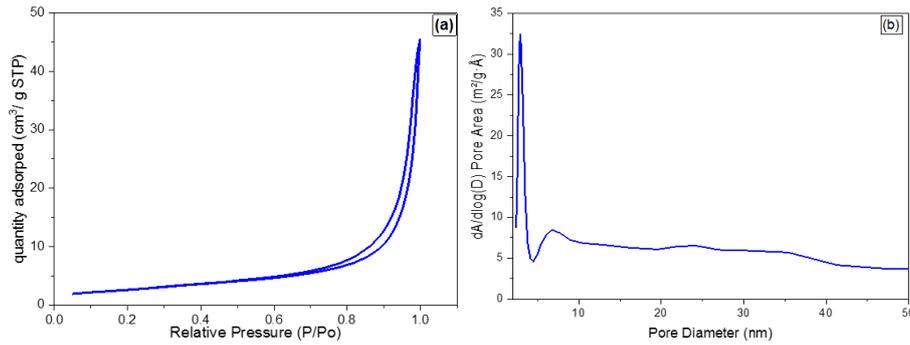
Fig. 3. (a) Nitrogen adsorption-desorption isotherm and (b) pore size distribution for BiOI.

The Uv-vis absorption curve of the as-prepared BiOI showed a wide range of absorbance-spectrum covering 220 to 650 nm with maxima at 232 in the Uv-region and another maximum in the visible region at 533nm (Fig. 4a). These results nominated the prepared BiOI nanoparticles as an excellent photocatalyst under natural sunlight. The energy-bandgap (E_g) calculation was conducted using Eq. 1, and it was found to be 1.9 eV [43-45]. This finding was within the E_g-range of the BiOI [23].

$$E_g = 1240 / \lambda_{AE} \tag{1}$$

where λ_{AE} is the edge wavelengths
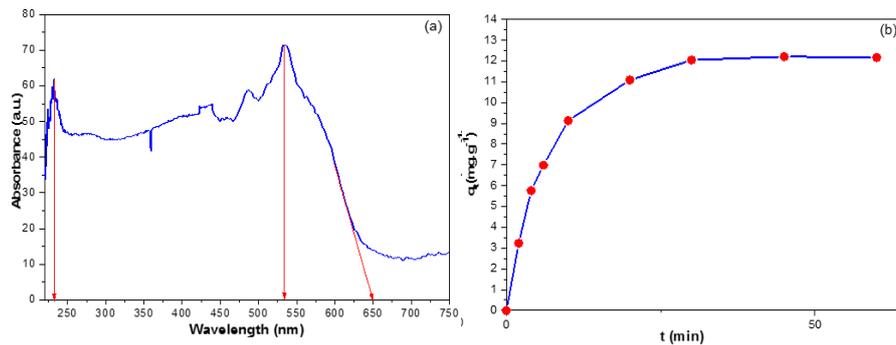
Fig. 4. (a) Absorbance spectrum for visible light by BiOI and (b) The contact time investigation for the adsorption of MG on BiOI.

3.2. Adsorption of malachite green

Fig. 4b represents the contact time investigation of MG on the prepared BiOI. The adsorbed quantity (q_t) was calculated using Eq. 2. The adsorption rate was investigated using the linearized pseudo-first-order (PFO) and pseudo-second-order (PSO) kinetic models expressed by Eq. 3 and Eq.4, respectively. The kinetic-rate-control-mechanism was studied by the liquid-film-diffusion-model (LFD) (Eq. 5) and the intraparticle-diffusion-model (IPD) (Eq. 6)[46, 47].

$$q_t = \frac{(C_o - C_t)\,V}{M}, \tag{2}$$

$$\ln(q_e - q_t) = \ln q_e - k_1.t \tag{3}$$

$$\frac{t}{q_t} = \frac{1}{k_2.q_e^2} + \frac{t}{q_e} \tag{4}$$

$$q_t = K_{IP} * t^{\frac{1}{2}} + C_i \tag{5}$$

$$\ln(1 - F) = -K_{LF} * t \tag{6}$$

where the factor $F = q_t/q_e$

where C_o, C_t, V and M were the initial concentration (mg.L^{-1}), unadsorped concentration (mg.L^{-1}), solution-volume (L), and sorbent-mass (g)

q_e (mg.g^{-1}) is the adsorbed amount of MG per gram of BiOI at equilibrium.

k_1(min^{-1}) and k_2 (g mg^{-1} min^{-1}) are the PFO-rate-constant and the PSO-rate-constant, respectively.

k_{ip} (mg g^{-1} min$^{-1/2}$) and k_{LF} (min^{-1}) are the IPDM-constant and LFDM- constant, respectively.

C_i: concentration in mg.g^{-1}.

The statistical parameters of MG adsorption on BiOI were calculated for the PFO and the PSO models (Fig.5 a and b). As presented in Table.1, the PSO model appeared to have the least residual sum of squires and reduced chi-squared values. Also, it had the highest correlation coefficient and an almost typical calculated q_e. The statistical parameters revealed a good agreement with the adsorption of MG on the BiOI for the PSO-model. The rate-control-mechanism for MG-adsorption on BiOI was studied by applying the intra-particle-diffusion (IPDM) and liquid-film-diffusion (LFDM) models as monitored in Fig 5c, d, and table 1. The K_{IP} value was six-times the K_{LF} value pointing to the preference of IPDM over the LFDM, but the high C_i value was opposite that prediction revealing a high boundary-layer resistance to IPDM [48]. The multi-linear-curve of IPDM and the statistical regression results of evident multi-control-mechanism on MG's adsorption by BiOI. This complexity may be due to the hetero-nature of the prepared BiOI to the difference in diffusion models.[49, 50].

Table 1. The parameters of kinetic order and the rate-controlling mechanisms
for MG adsorption on BiOI nanoparticles.

Adsorption kinetic order						
Pseudo-first-order kinetic model				**Pseudo-second-order kinetic model**		
q_e exp. (mg. g^{-1})	q_e cal. (mg. g^{-1})	k_1	R^2	q_e cal. (mg. g^{-1})	k_2	R^2
12.218	2.408	0.021	0.231	13.793	0.02	0.998
Adsorption kinetic rate control mechanism						
Intraparticle diffusion model			**Liquid film diffusion model**			
K_{id} (mg/g min1/2)	C (mg/g)	R2	K_{fd} (min–1)		R^2	
0.907	5.798	0.954	0.024		0.389	
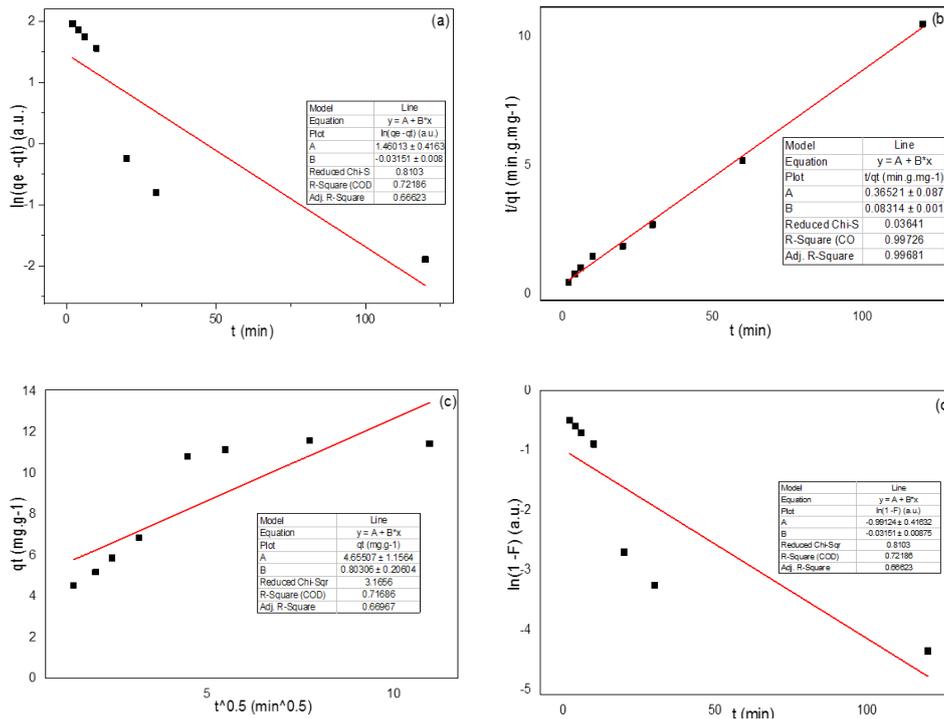
Fig. 5. (a) pseudo-first-order model, (b) pseudo-second-order model, (c) intraparticle-diffusion model and (d) liquid-film-diffusion model kinetic investigations for the MG adsorption on BiOI.

3.3. Photocatalytic degradation of malachite green

The photocatalytic electrons may react with O_2 or OH^- producing the reactive radicals of oxygen or hydroxyl ion, respectively. The former requires -0.33 eV, while the second requires $+1.9$ eV, which can be provided by BiOI photocatalyst; this corresponds to what had been proved that the hydroxyl has the most impact in the degradation-process when using BiOI-photocatalyst [51-53]. The MG degradation by BiOI was investigated, and the process was monitored by determining the absorbance at 611 nm for the picked aliquotes (Fig 6a). The kinetics of the MG-photodegradation by BiOI under sunlight was studied using the first-order-kinetic-model expressed by Eq. 7.

$$\ln \frac{C_t}{C_0} = kt \tag{7}$$

where
C_0: MG initial concentration
C_t: MG remained concentration at t min
K: the first-order-rate-constant

The plot of Eq. 7 was monitored in Fig. 6b from-which the rate constant was calculated. The rate-constant was found to be 2.2 x10^{-2} min^{-1}, which was good enough for the photocatalytic degradation system to achieve 96% degradation-efficiency within three hours. These findings can be considered good compared to previous literature [54, 55]. For the reusability of the photocatalyst was performed for three times. The solution was filtered and the photocatalyst was dried at 105oC for 1h. The dried BiOI was weighed, transferred to a 200 ml beaker and the MG solution was added in a proper volume to conserve the ratio of photocatalyst: solution. The beaker was shaken for 1h in absence of light after which it was placed under the sunlight. The BiOI showed consistent performance during the further three durations with each batch of the fresh MG pollutant as monitored in Fig. 7.
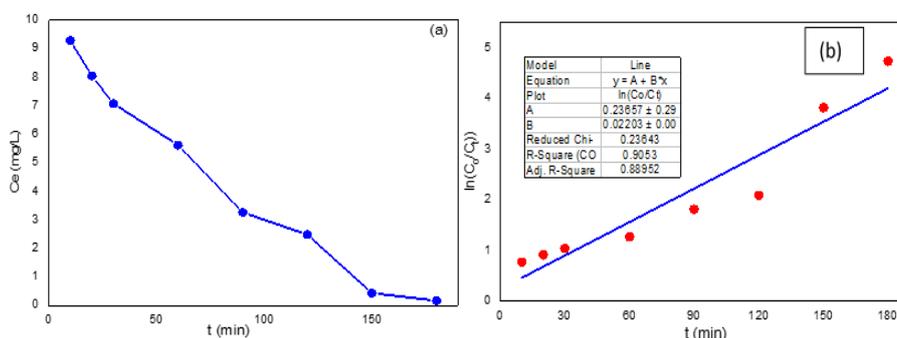
Fig. 6. (a) degradation trend and (b) 1st-order kinetic investigation for the MG photocatalytic degradation under sunlight by BiOI-photocatalyst.
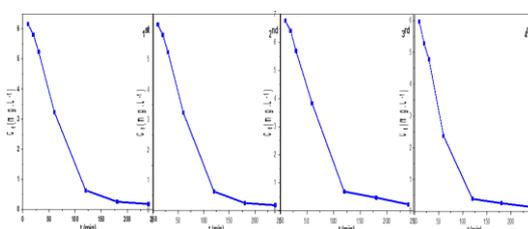
Fig. 7. Reusability of the prepared BiOI nanoparticles for the photodegradation of MG in water.

4. Conclusion

BiOI nanoparticles were fabricated successfully by a simple-refluxing-method. The method succeeded in the preparation of nanoscale-BiOI particles. The adsorption of MG as a model of organic pollutants on BiOI followed the PSOM with a relatively-fast equilibrium time having an adsorption capacity of 12.1 mg. g^{-1}. The MG photodegradation by BiOI under natural sunlight fitted the PFO kinetic-model with 98% degradation efficiency in three hours. Furthermore, the as-prepared BiOI-photocatalyst was found to be a magnificent photocatalyst for organic pollutants using free sunlight energy.

References

[1] N. Sedaghati et al., Boosted visible-light photocatalytic performance of TiO2-x decorated by BiOI and AgBr nanoparticles, **384**, 112066 (2019).
[2] J. Kong et al., Perovskite-based photocatalysts for organic contaminants removal: Current status and future perspectives, **327**, 47 (2019).
[3] A. Sintakindi, B. Ankamwar, Environmental Technology Reviews **10**(1), 26 (2021).
[4] R. Argumedo-Delira, M. J. Gómez-Martínez, R. Uribe-Kaffure, Applied Sciences **11**(1), 448 (2021).
[5] S. S. Ali et al., Journal of Hazardous Materials **403**, 123575 (2021).
[6] N. S. Topare, S. A. Bokil, Materials Today: Proceedings, 2021.
[7] A. Yurtsever et al., Science of The Total Environment **751**, 141572 (2021).
[8] Q. Feng et al., Chemosphere **262**, 128416 (2021).
[9] M. H. D. Othman et al., Advanced Membrane Technology for Textile Wastewater Treatment, in Membrane Technology Enhancement for Environmental Protection and Sustainable Industrial Growth, Springer, 91 (2021).

64

[10] G. Parshetti et al., Biodegradation of Malachite Green by Kocuria rosea MTCC 1532. 2006. **53**(4).

[11] S. Srivastava, R. Sinha, D. J. A. T. Roya, Biodegradation of Malachite Green by Kocuria rosea MTCC 1532. 2000. **66**, 319 (2000).

[12] P. Arabkhani, A. J. J. O. H. M. Asfaram, Development of a novel three-dimensional magnetic polymer aerogel as an efficient adsorbent for malachite green removal, **384**, 121394 (2020).

[13] M. A. Adebayo et al., Removal of aqueous Congo red and malachite green using ackee apple seed–bentonite composite, **38**, 100311 (2020).

[14] Y. Yulizar, D. O. B. Apriandanu, R. I. J. C. P. L. Ashna, La2CuO4-decorated ZnO nanoparticles with improved photocatalytic activity for malachite green degradation, **755**, 137749 (2020).

[15] S. I. El-Hout et al., Highly efficient sunlight-driven photocatalytic degradation of malachite green dye over reduced graphene oxide-supported CuS nanoparticles, **849**, 156573 (2020).

[16] R. Haounati et al., Elaboration and properties of a new SDS/CTAB@ Montmorillonite organoclay composite as a superb adsorbent for the removal of malachite green from aqueous solutions, **255**, 117335 (2020).

[17] J. Song et al., Pathway and kinetics of malachite green biodegradation by Pseudomonas veronii, **10**(1), 1 (2020).

[18] I. D. Mall et al., Adsorptive removal of malachite green dye from aqueous solution by bagasse fly ash and activated carbon-kinetic study and equilibrium isotherm analyses, **264**(1-3), 17 (2005).

[19] X. Hu et al., Step-scheme NiO/BiOI heterojunction photocatalyst for rhodamine photodegradation, **511**, 145499 (2020).

[20] W. Liu et al., Dual Z-scheme g-C3N4/Ag3PO4/Ag2MoO4 ternary composite photocatalyst for solar oxygen evolution from water splitting, **456**: 369 (2018).

[21] H. Ran et al., Enhanced performances of dye-sensitized solar cells based on Au-TiO2 and Ag-TiO2 plasmonic hybrid nanocomposites, **430**, 415 (2018).

[22] J. Wang et al., ZnO nanoparticles implanted in TiO2 macrochannels as an effective direct Z-scheme heterojunction photocatalyst for degradation of RhB, **456**, 666 (2018).

[23] L. Zeng et al., Preparation of interstitial carbon doped BiOI for enhanced performance in photocatalytic nitrogen fixation and methyl orange degradation, **539**, 563 (2019).

[24] Y. Li et al., Efficient decomposition of organic compounds and reaction mechanism with BiOI photocatalyst under visible light irradiation, **334**(1-2), 116 (2011).

[25] P. Intaphong et al., Sonochemical synthesis and characterization of BiOI nanoplates for using as visible-light-driven photocatalyst, **213**, 88 (2018).

[26] X. Chang et al., Photocatalytic degradation of PCP-Na over BiOI nanosheets under simulated sunlight irradiation, **10**(15), 1957 (2009).

[27] J.-H. Peng et al., Rapid microwave-assisted solvothermal synthesis and visible-light-induced photocatalytic activity of Er3+-doped BiOI nanosheets **29**(5), 1158 (2018).

[28] A. Luz, C. J. S. S. S. Feldmann, Phase-transfer assisted synthesis of BiOI nanoplatelets, quantum-confined color and selective modification of surface conditioning, **13**(5), 1017 (2011).

[29] W. Wang et al., Visible-light-responsive photocatalysts xBiOBr–(1− x) BiOI, **9**(1), 8 (2008).

[30] M. Elamin et al., Preparation of Large Carbon Nanofibers on a Stainless Steel Surface and Elucidation of their Growth Mechanisms, **74**(3), 253 (2019).

[31] F. Gao et al., Physical Chemistry Chemical Physics **14**(30), 10572 (2012).

[32] J.-M. Song et al., CrystEngComm **12**(11), 3875 (2010).

[33] W. W. Lee et al., RSC Advances **5**(30), 23450 (2015).

[34] Z. Deng et al., From bulk metal Bi to two-dimensional well-crystallized BiOX (X= Cl, Br) micro-and nanostructures: synthesis and characterization, **8**(8), 2995 (2008).

[35] S.-Y. Chou et al., Novel synthesis of bismuth oxyiodide/graphitic carbon nitride nanocomposites with enhanced visible-light photocatalytic activity, **6**(40), 33478 (2016).

[36] C.-C. Chen et al., Bismuth oxyfluoride/bismuth oxyiodide nanocomposites enhance visible-light-driven photocatalytic activity. Journal of colloid and interface science, **532**, 375 (2018).

[37] M. Thommes et al., Physisorption of gases, with special reference to the evaluation of surface

area and pore size distribution (IUPAC Technical Report), **87**(9-10), 1051 (2015).

[38] Z. Yang et al., Preparation and Properties of BiOI with High Sorption Capacity, **35**(3), 620 (2020).

[39] J. Yang et al., Facile Synthesis of Kermesinus BiOI with Oxygen Vacancy for Efficient Hydrogen Generation, 127607 (2020).

[40] X. Hao et al., The preparation of full-range BiOBr/BiOI heterojunctions and the tunability of their photocatalytic performance during the synthesis of imines under visible light irradiation, **528**, 147015 (2020).

[41] H. Zhang et al., Microwave-Aided Synthesis of BiOI/g-C3N4 Composites and Their Enhanced Catalytic Activities for Cr (VI) Removal, 138143 (2020).

[42] S. Bargozideh et al., Effect of carbon nanotubes loading on the photocatalytic activity of BiSI/BiOI as a novel photocatalyst, **27**(29), 36754 (2020).

[43] M. Mehrali-Afjani, A. Nezamzadeh-Ejhieh, H. J. C. P. L. Aghaei, A brief study on the kinetic aspect of the photodegradation and mineralization of BiOI-Ag3PO4 towards sodium diclofenac, **759**, 137873 (2020).

[44] N. Jeevanantham, O. J. J. O. T. I. C. S. Balasundaram, High-performance visible light photocatalytic activity of cobalt (Co) doped CdS nanoparticles by wet chemical route **16**(2), 243 (2019).

[45] M. Sabonian, K. J. I. J. O. C. Mahanpoor, Preparation of ZnO nanocatalyst supported on todorokite and photocatalytic efficiency in the reduction of chromium (VI) pollutant from aqueous solution, **9**(3), 201 (2019).

[46] M. R. Elamin, B.Y. Abdulkhair, A.O. Elzupir, Scientific reports **9**(1), 1 (2019).

[47] J. Acharya et al., Chemical Engineering Journal **149**(1-3), 249 (2009).

[48] S. Debnath, U. C. J. D. Ghosh, Equilibrium modeling of single and binary adsorption of Cd (II) and Cu (II) onto agglomerated nano structured titanium (IV) oxide, **273**(2-3), 330 (2011).

[49] S. Markandeya, G. J. R. J. E. T. Kisku, Linear and non-linear kinetic modeling for adsorption of disperse dye in batch process, **9**(6), 320 (2015).

[50] B. Hameed, R. Krishni, S. J. J. O. H. M. Sata, A novel agricultural waste adsorbent for the removal of cationic dye from aqueous solutions, **162**(1), 305 (2009).

[51] J. Wen et al., Applied surface science **391**, 72 (2017).

[52] C. Wang,X. Zhang, Y. Liu, Applied Surface Science **358**, 28 (2015).

[53] D. Jiang et al., Dalton Transactions **42**(44), 15726 (2013).

[54] A. Modwi et al., Digest Journal of Nanomaterials & Biostructures (DJNB) **14**(2), 2019.

[55] S. Bargozideh, M. Tasviri, M. Ghabraei, Environmental Science and Pollution Research **27**(29), 36754 (2020).